IEEE Access
Multidisciplinary | Rapid Review | Open Access Journal

Received 13 May 2022, accepted 20 June 2022, date of publication 30 June 2022, date of current version 12 July 2022.

Digital Object Identifier 10.1109/ACCESS.2022.3187433

RESEARCH ARTICLE

Mutual Coupling Reduction in Closely Spaced MIMO Dielectric Resonator Antenna in H-Plane Using Closed Metallic Loop

MANZOOR ELAHI[1], (Member, IEEE), AMIR ALTAF[2], (Member, IEEE), EQAB ALMAJALI[3], (Member, IEEE), AND JAWAD YOUSAF[4]

[1]School of Electrical and Electronic Engineering, Chung-Ang University, Heukseok-dong, Dongjak-gu, Seoul 06974, Republic of Korea
[2]Department of Electrical and Computer Engineering, Sungkyunkwan University, Suwon 440-746, South Korea
[3]Electrical Engineering Department, University of Sharjah, Sharjah, United Arab Emirates
[4]Department of Electrical, Computer and Biomedical Engineering, Abu Dhabi University, Abu Dhabi, United Arab Emirates

Corresponding authors: Jawad Yousaf (jawad.yousaf@adu.ac.ae) and Manzoor Elahi (manzoorelahi19@gmail.com)

This work was supported by Abu Dhabi University's Office of Research and Sponsored Programs.

ABSTRACT In this study, the mutual coupling in multiple-input-multiple-output (MIMO) dielectric resonator antenna (DRA) is reduced by employing closed metallic loops. The loops are wrapped around the adjacent edges of the dielectric resonators (DR) where magnetic coupling is significant. The proposed method employs only the conductive metallic strips for mutual coupling reduction and this makes the entire design very simple and compact. The impedance bandwidth varies from 4.73 to 5.1 GHz, covering the Sub–6 GHz 5G band. The realized MIMO DRA has an isolation of 28 dB at the resonant frequency with a measured peak gain at each port of 3.5 dBi and a peak radiation efficiency of 93%. The obtained measured results yield a low correlation coefficient (< 0.05) mostly at the entire band that contribute to diversity gain (> 9.8 dB) to increase the capacity of communication system, is reported in this paper. The proposed antenna was fabricated and the closed loop strip is wrapped around using in house facility. Furthermore, some issues related to the fabrications tolerance have been investigated to justify the difference between some simulated and measured results.

INDEX TERMS Dielectric resonator antenna, multiple input multiple output, isolation, envelope correlation coefficient, mean effective gain, quality factor, eigenmode analysis.

I. INTRODUCTION

During the recent years, there has been a rapid development in communication technology in terms of massive information exchange and high data rates. At the antenna side, this is mostly deployed using MIMO technology. Although MIMO antennas provide high data rates and speed over multipath channels, high coupling between radiating elements can affect a MIMO antenna diversity. Therefore, high isolation among radiating elements is required to realize the MIMO diversity system [1], [2]. A lot of research has been done on MIMO antennas, that use a patch as a radiating element due to the ease of manufacturing. However, MIMO antennas that use DRs, as radiating elements, have several advantages over those comprised of conventional microstrip patches. As the DRA is purely made of a dielectric material, it has much lower conductivity losses, much better radiation efficiency, and wider bandwidth [3], and owns good temperature stability [4]. The low loss property, in particular, makes it a better candidate for MIMO design at high frequencies.

Previously, numerous techniques were utilized to improve isolation between the DRAs. In one study [5], a metasurface shield consisting of 1×7 split ring resonator (SRR) unit cells, is used between two DRA elements to improve the isolation by 30–46.5 dB in the frequency band of 59.3–64.8 GHz. Surface waves are the main reason for increasing mutual coupling, therefore an electromagnetic bandgap (EBG) structure in [6] is placed between two patch antennas to

The associate editor coordinating the review of this manuscript and approving it for publication was Luyu Zhao.

reduce the mutual coupling up to −29.5 dB at 5.6 GHz. Similarly, an EBG structure in [7] provides an isolation of 17–35 dB between the DRA elements over a frequency span of 57–64 GHz. In another study [8], a simple ring-shaped defected ground structure (DGS) is etched from the ground, which suppresses the mutual coupling between the two DR elements to −17 dB around 3.3 GHz. A spiral ring resonator is proposed in [9] to act as a band rejection filter to reduce the mutual coupling to −25 dB at 6.56 GHz between the two square DRs. Isolation can also be enhanced by utilizing the artificial magnetic conductor (AMC) as reported in [10]. The level of isolation was improved to 35 dB at 10 GHz. Frequency selective surface (FSS) wall is employed in [11] to block the field between the DRA elements. This resulted in a mutual coupling reduction to –30 dB in the desired band of 57–63 GHz. Another decoupling mechanism presented in [12] is utilizing a dielectric superstrate above the MIMO DRA. The coupling fields inside the DRAs are affected by the superstrate through electromagnetic fields interaction that isolate the elements by 25 dB. A method based on combining a DGS slot and metallic strips on the top substrate is proposed in [13]. Comparatively, this method occupies less space than DGS and isolate the MIMO elements by 22 dB. Although the above techniques reduce the coupling significantly, the overall design became bulky due to the use of a periodic structure. Other studies [14–16] involve the generation of orthogonal modes by complex hybrid feeding mechanism. Similarly, a hybrid isolator in [17] comprises an EBG structure and milli-meter wave choke absorber is utilized to achieve isolation varies from 29 to 49 dB. In [18], metal strips were printed on the upper surface of the DRAs to increase isolation. The isolation being achieved is 25–28 dB in the entire bandwidth of 27.5–28.35 GHz. Another method in [19] isolates the MIMO DRA elements by 45 dB at the design frequency without using the decoupling structure. This method is based on the excitation of the high order modes in the DRA that are unable to reach the feeding port. In [20], a MIMO DRA with an isolation level of 25 dB at 15 GHz is reported by using the metallic strips on the lateral walls of the DRA elements. The isolation mechanism is very simple and compact. The MIMO elements are magnetically coupled. The coupling fields in the DRA are pushed away by the strips printed on the lateral walls. However, the isolation of the field in the middle region of the adjacent walls of the DRA is not highlighted properly. Similarly, coupling in [21] has been reduced in the E-plane by printing multiple metallic strips on the DRA elements. Although simulated isolation of 50 dB has been achieved at 25.8 GHz, the work lacks important details about the isolation mechanism. Furthermore, these multiple strips deviate the radiation pattern from the broadside direction by 45° in $\phi = 90°$ plane.

In this paper, a very simple technique is proposed to achieve high isolation between DRA elements in the H-plane. The proposed technique is based on the use of closed metallic loops printed on the adjacent edges of the two DRAs in such a way that makes them shorted to the ground. This technique is very simple like [18] and [20] and does not need an extra footprint or increase the height of the MIMO DRA. The significant feature of the proposed isolation technique is that the overall design is very compact, i.e., the inter-element distance is $g = 1$ mm $= 0.016\lambda_0$ while it provides a very good isolation performance as low as 50 dB. This work also provides a detailed study on the isolation mechanism and its sensitivity analysis. Furthermore, the fabrication tolerance and its impact on the performance of the MIMO are addressed here. For this purpose, two prototypes of the MIMO DRA are fabricated to verify the fabrication tolerance of the metallic strips on the DRAs and the measured results are compared to the simulated ones for validation. The impedance bandwidth of the proposed MIMO DRA spans from 4.73 GHz to 5.1 GHz with measured isolation of 28 dB at the design frequency. The peak gains of 3.5 dBi and radiation efficiency of more than 93% are noticed for each port. The farfield envelope correlation coefficients lies below 0.05 in the bandwidth with the diversity gain greater than 9.8 dB. Finally, the simulated mean effective gains are in good agreement with the measured results.

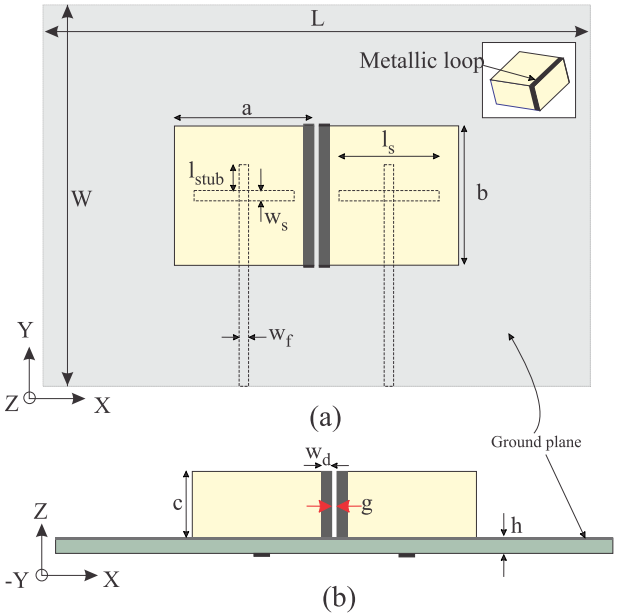

FIGURE 1. Geometry of the proposed MIMO DRA: (a) Top view. (b) Side view. $[a = b = 20, d = 8.15, g = 1, l_s = 16.7, w_s = 1.5, w_f = 3.43, w_d = 2, l_{stub} = 6.07, h = 1.52, L = 120, W = 70,]_{mm}$.

II. DESIGN OF THE PROPOSED DRA

Fig. 1 shows the configuration of the proposed MIMO DRA. Two identical rectangular dielectric resonators (DRs) made up of Alumina ($\tan\delta = 0.0001$, and $\epsilon_r = 9.9$) with dimensions of $a \times b \times c$ and an inter-element spacing g are placed directly above the ground plane. Two slots with each of length l_s and width w_s are etched from the ground plane. Each DR is fed at the center by a microstrip line that is placed on the bottom layer of Taconic TLY-5 ($\tan\delta = 0.0009$,

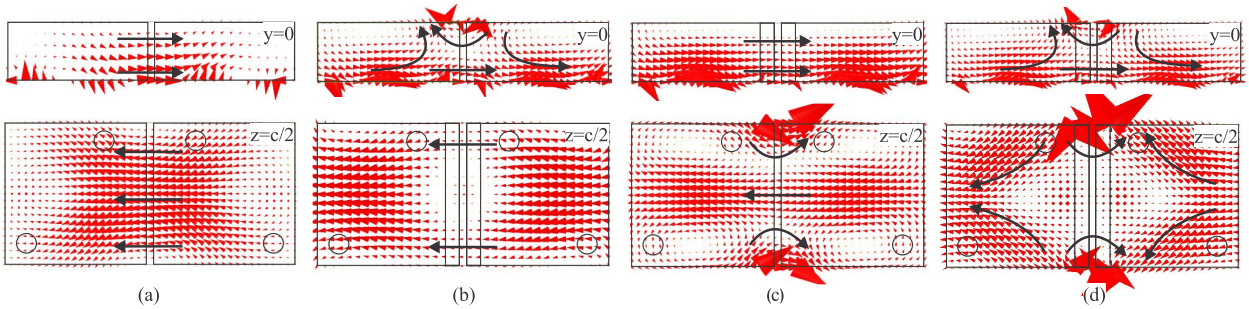

FIGURE 2. Magnetic field visualization in MIMO DRA at 4.9 GHz: (a) Conventional (MIMOI). (b) MIMO with strips printed on the top surface (MIMO2). (c) MIMO with strips printed on the lateral walls (MIMO3). (d) Proposed MIMO (MIMO4).

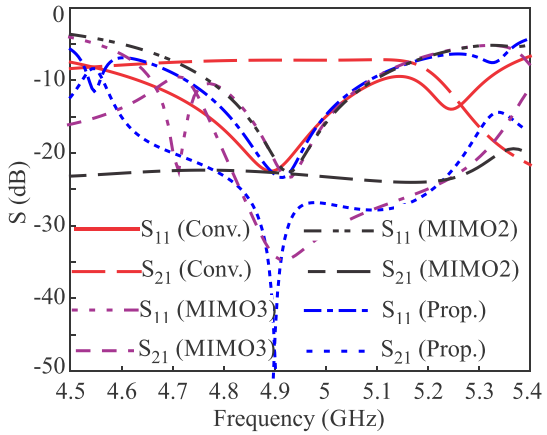

FIGURE 3. Performance comparison of the four types of MIMO DRAs in terms of simulated S-parameters.

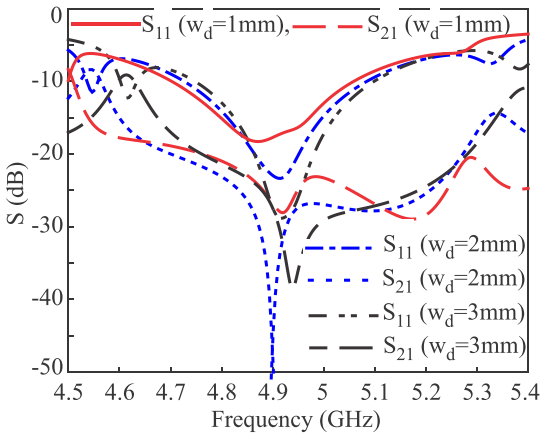

FIGURE 4. S-parameters of the MIMO4 for different values of w_d.

$\epsilon_r = 2.2$). To improve the isolation between the DR elements, a rectangular metal strip of width w_d is printed on the adjacent edge of each DR element that is shorted from both ends to the ground, making a closed loop. The simulations are carried out in the HFSS.

III. DECOUPLING STRUCTURE (MECHANISM AND SENSITIVITY ANALYSIS)

To explain the decoupling mechanism of the proposed design, the magnetic field distribution for MIMO1 (conventional), MIMO2 (with strips on the top surface), MIMO3 (with strips on the lateral walls), and MIMO4 (Proposed) are shown in Fig. 2, in two planes: $y = 0$ and $z = c/2$. In the case of conventional MIMO in Fig. 2(a), the magnetic fields are aligned in the DRA elements of MIMO1 in both planes, which results in significant coupling. Fig. 2(b) explains the isolation in the MIMO2 due to the strips on the top surface of the DRA. The strips generate the magnetic fields in the direction opposite to the coupling fields between the DRA elements. Therefore, the coupling due to the field in the center of the DRA is reduced. However, the top strips do not prevent the coupling fields near the lateral walls of the DRA as shown in $z = c/2$ plane. The coupling due to the fields near the lateral walls can be reduced by printing the strips on the lateral walls (MIMO3) given in Fig. 2(c). The $z = c/2$ plane clearly depicts that fields of the strips do not permit the field of the DRA to couple near the side walls, but, the fields of the DRA in the $y = 0$ plane still exist to couple. The fields in $y = 0$ plane as well as near the lateral wall can be greatly reduced by utilizing a closed metallic loop on the edges of the adjacent wall of the DRA elements. Fig. 2(d) shows the magnetic field distribution of the proposed structure, which has excellent isolation in $y = 0$ and $z = c/2$ planes. The performance of the four cases of the MIMO in terms of S-parameters is compared in Fig. 3. In case of conventional MIMO the isolation level is above 10 dB at the resonance frequency of 4.9 GHz, due to closely spaced elements. The isolation is improved in MIMO2 and MIMO3, which is 23 dB and 33 dB, respectively. Whereas, the proposed structure has superior performance that is 50 dB at the resonance frequency.

It is important to note that the width (w_d) of the decoupling strips is shown to affect the performance of the MIMO DRA as exhibited in Fig. 4. It is evident that by changing w_d value, the isolation level varies. This stems from the fact that the width of the strip controls the inductance defined by the strip and hence it affects the generated magnetic field intensity across the coupling area between DRAs. Another parameter that should be considered is the inter-element spacing g. The isolation level does not remain the same as g varies. Fig. 5 plots S-parameters for different values of g. Poor performance is realized for the values of g other than 1 mm as the current design is optimized at g =1 mm. However, this

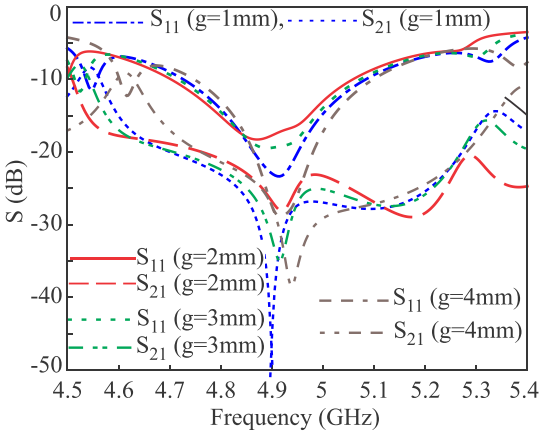

FIGURE 5. S-parameters of the MIMO4 for different values of *g*.

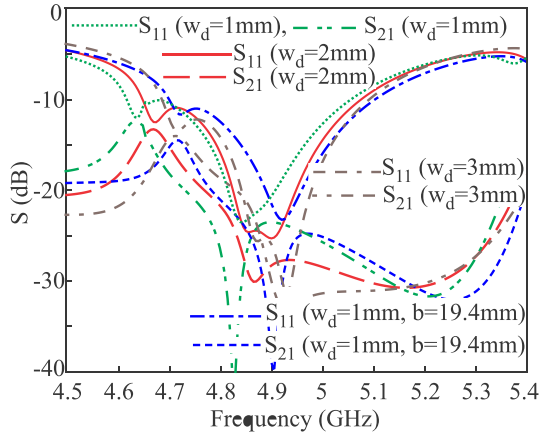

FIGURE 6. Optimized and non-optimized S-parameters of MIMO4 with $g = 3$mm. [For optimized design: $[b = 19.4, w_d = 1]_{mm}$].

technique is useful at any inter-element spacing. To realize this, some design parameters need to be optimized. For illustration, at g =3 mm, a high isolation performance is achieved at 4.9 GHz by changing the values of parameters w_d and b to 1 mm and 19.4 mm, respectively, as depicted in Fig. 6. Conventionally, the isolation should increase by increasing g but contradictory results are realized in Fig. 5. From this study, it is concluded that the isolation performance of the closed loops are dependent on the value of g as well as w_d. Fig. 7 shows the E-field distribution in the MIMO DRA with and without metallic loops using eigenmode simulation versus driven model simulation. It was observed that the fundamental mode (TE^x_{111}) is the closest mode to the resonance frequency. The calculated quality factor (Q-factor) for the said mode, with and without metallic loop carried out in eigenmode simulation setup [22], [23], are 9247 and 11924, respectively. The low Q-factor, obtained in the case of metallic loop, is caused by the additional losses in the strip's copper material.

IV. MEASURED RESULTS AND DISCUSSION

A prototype-I (Prot–I) of the MIMO DRA is fabricated as shown in Fig. 8(a). Both the DRAs were attached to

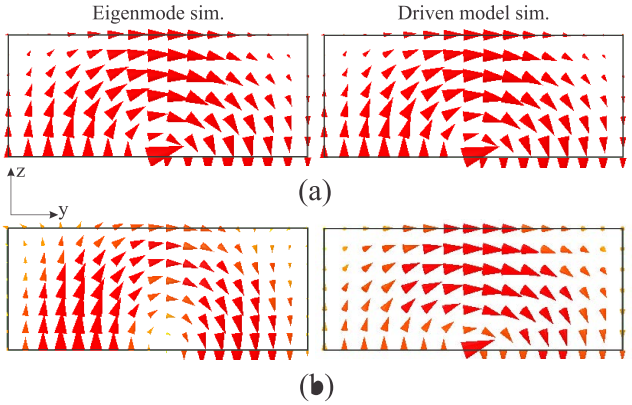

FIGURE 7. Simulated E-field distribution of fundamental mode: (a) Eigenmode simulation at $\angle 90°$ and driven model simulation at $\angle -90°$ in MIMO DRA Without metallic loop. (b) Eigenmode simulation at $\angle -80°$ and driven model simulation at $\angle 0°$ in MIMO DRA With metallic loop.

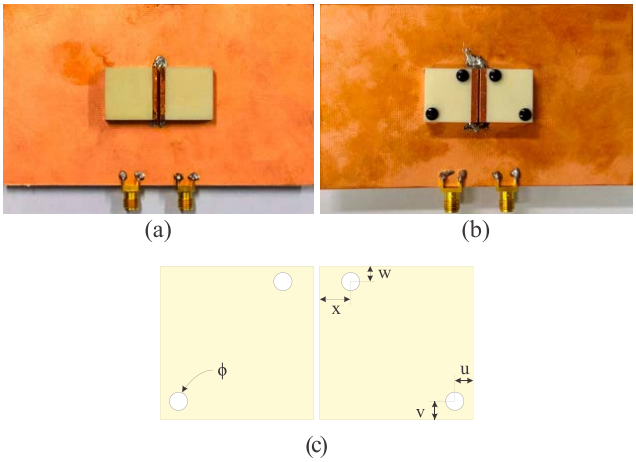

FIGURE 8. Images of the two prototypes: (a) Prot–I. (b) Prot–II. (c) DRAs with holes. $[u = v = 3, w = 2.8, x = 6, \phi = 2.5]_{mm}$.

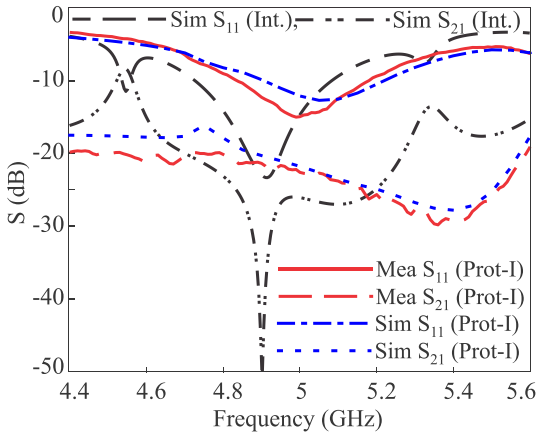

FIGURE 9. Comparison of the simulated and measured S-parameters of Prot–I.

the ground plane using a layer of glue. The measured and simulated S-parameters of Prot–I are compared with the initial simulations (MIMO4) given in Fig. 9. It can be seen that the resonance frequency is shifted to 5 GHz while the isolation minima shifted to 5.4 GHz. We believe that the gap

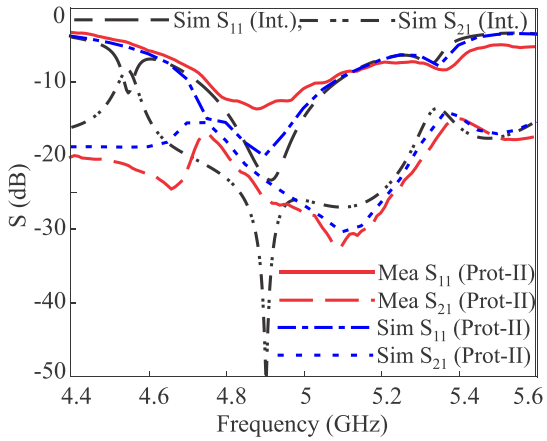

FIGURE 10. Comparison of the simulated and measured S-parameters of Prot–II.

due to glue between the DRA and the ground reduces the overall permittivity hence, it causes the radiating structure to resonate at a higher frequency. For verification, the gap of 25 μm is added in the simulation model between the ground and DRAs as well as between decoupling strips and DRAs. The simulation results confirmed this inference. Next, some changes were made to the Prot–I to overcome the air gap between the DRA and ground. A pair of polycarbonate screws were inserted into the DRAs by making the holes through them as shown in Fig. 8(b) termed as Prototype–II (Prot–II). This creates a firm contact with the ground and hence may reduce the frequency shift observed in Prot-I. The location of the holes in the DRAs is shown in Fig. 8(c). The results of the Prot–II were measured and compared with the initial simulations (MIMO4) as depicted in Fig. 10. Now, the MIMO is resonating at 4.9 GHz, whereas the isolation minima is located at 5.08 GHz. Further investigations were made in simulations by assuming the gap between the DRA and the decoupling strips around 25 μm with no gap between the DRA and the ground. The simulated and measured results for isolation agree very well under this assumption. In conclusion, it was found that the shift in the isolation minima is very sensitive to the air gap between the DRA and decoupling strips. Thus, the screws improved the results as they reduced the gap between the DRA and the ground, however, precise fabrication is needed to remove the gap between the DRA and metallic strip completely. Therefore, if the strips are printed properly such that no gap exists, the measured results would ultimately match with the initial simulations. Fig. 11 shows the farfield measurement setup of the fabricated MIMO DRA. The co- and cross-polarization radiation patterns of the MIMO DRA in $\phi = 0°$ and $\phi = 90°$ planes for Port-I and Port-II are depicted in Fig. 12 at the center frequency of 4.9 GHz. It is noticed that the measured results agree well with the simulated results. The co-pol patterns in $\phi = 0°$ plane for the two ports are slightly tilted in opposite directions, whereas the orientations of the patterns in $\phi = 90°$ plane are similar for both ports. Furthermore, the x-pol levels in the broadside direction are

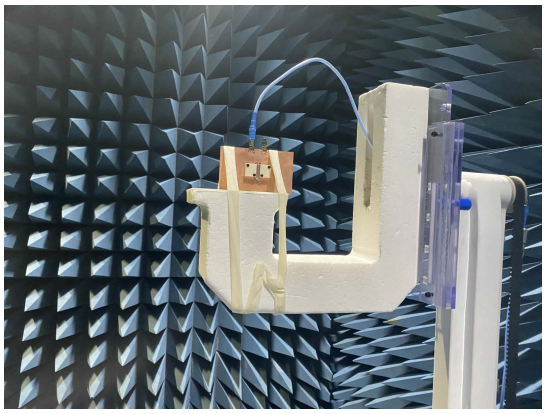

FIGURE 11. Farfield measurement environment of the MIMO DRA.

around -10 dB, which are less than the co-pol by 11 dB to 13.5 dB in both planes. The farfield realized gain and radiation efficiencies of Port-I and Port-II are shown in Fig. 13 in the broadside direction. Both the measured and simulated gain curves agree well within the bandwidth of interest. The peak gain achieved for both ports is 3.5 dBi and the radiation efficiency of 93%. Diversity gain (DG) and envelope correlation coefficient (ECC) from the S-parameters and farfield radiation patterns are given in Fig. 14. The ECC shows how the radiation patterns of the elements in MIMO system are independent. The ECC of the MIMO DRA is calculated from the S-parameters by using the following equation [24]:

$$ECC = \frac{|S_{11}^* S_{12} + S_{21}^* S_{22}|}{(1 - (|S_{11}|^2 + |S_{21}|^2))(1 - (|S_{22}|^2 + |S_{12}|^2))} \quad (1)$$

whereas the ECC from the farfield is given by equation [25]:

$$ECC = \frac{|\iint_{4\pi}[E_1(\theta,\phi) * E_2(\theta,\phi)]d\Omega|^2}{\iint_{4\pi}|E_1(\theta,\phi)|^2 d\Omega \iint_{4\pi}|E_2(\theta,\phi)|^2 d\Omega} \quad (2)$$

Simulated ECC obtained from the S-parameters and farfield patterns are close to each other in the desired bandwidth, however, the measured ECC is a bit higher than the simulated one in the band of interest. ECC has to be 0 ideally but in a practical environment, the acceptable limit of ECC is less than 0.5. In our case the measured ECC is below 0.05. Similarly, for a reliable wireless system, the value of DG has to be as high as 10 dB in the operating bandwidth. The diversity gain is calculated from the ECC by the following equation [26]:

$$DG = 10\sqrt{1 - |ECC|^2} \quad (3)$$

Based on the measured values of the ECC, the DG is greater than 9.8 dB in the desired band. Another important parameter is the mean effective gain (MEG) of the MIMO DRA. It provides the gain performance under the environmental effects and can be seen as the ratio of received power at a diversity antenna to the received power at an isotropic antenna. MEG analysis is done at Port-I and Port-II in Fig. 15. Both the simulated and measured results agree

TABLE 1. Comparison of the proposed work with earlier studies.

Ref.	Technique	Design frequency (GHz)	E–E distance (λ_0)	Isolation (dB)	ECC	Area/Volume occupied by isolating structure (λ_0^2 or λ_0^3)	Merits or Demerits of isolating structure
[5]	Metasurface shield	60	0.2	30 to 46.5	–	$1.96 \times 0.28 \times 0.05$	increase height
[6]	EBG structure	5.6	1.045	29.5	–	1.13×0.84	increase footprint
[8]	DGS	3.3	0.5	17	–	NA	–
[9]	Spiral resonator	6.56	0.11	25*	–	$0.2 \times 0.18 \times 0.022$	increase height
[10]	AMC	10	0.5	35*	–	1×1	increase footprint
[11]	FSS wall	60	–	30	5e−6	$1.52 \times 0.38 \times 0.1$	increase height
[12]	Dielectric superstrate	10	0.166	35	Near to 0	$3 \times 1.66 \times 0.69$	increase height
[18]	Metal strip on DR	28	0.14	27	0.013	No extra space	Simple design
[19]	High order modes	5.25	0.1	28	–	No isolator used	Simple design
[20]	Grounded strips on the lateral walls of DRs	15	0.005	28*	–	No extra space	Simple and compact design
[21]	E-shaped and I-shaped strips on adjacent surfaces and farther edges	26	0.0866	50*	–	No extra space	Simple and compact design
[Prop.]	Close loop	4.9	0.016	28	<0.05	No extra space	Simple and compact design

*: represents the simulated values only.

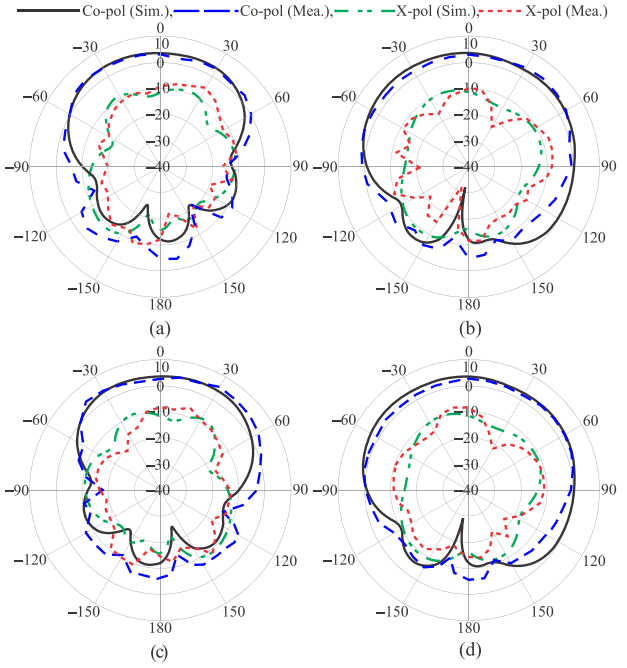

FIGURE 12. Comparison of the simulated and measured radiation patterns at 4.9 GHz: (a) $\phi = 0°$ plane (Port-I). (b) $\phi = 90°$ plane (Port-I). (c) $\phi = 0°$ plane Port-II. (d) $\phi = 90°$ plane (Port-II).

well with each other. The ratio MEG-I/MEG-II should be less than 3 dB. The simulated MEG is based on the following equations [27]:

$$MEG_i = 0.5[1 - |S_{ii}|^2 - |S_{ij}|^2] \quad (4)$$

$$MEG_j = 0.5[1 - |S_{ij}|^2 - |S_{jj}|^2] \quad (5)$$

Table 1 summarizes the comparison of the proposed structure with earlier studies. Metasurface shield, spiral resonator, FSS wall and dielectric superstrate are used for isolation in MIMO elements in [5], [9], [11] and [12], respectively. The drawback of these techniques is the increase in the height of overall structure. Similarly, EBG, DGS

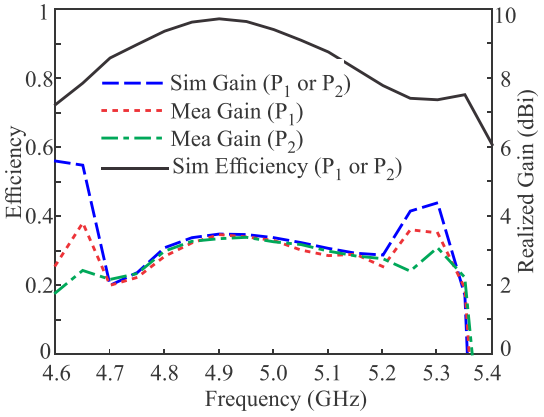

FIGURE 13. Comparison of the simulated and measured broadside realized gain and simulated efficiency of Port-I and Port-II.

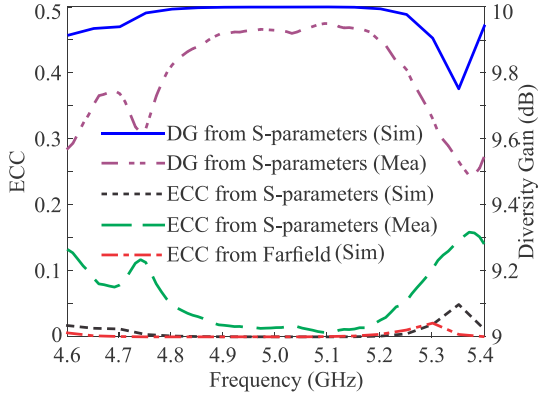

FIGURE 14. Envelope correlation coefficient and diversity gain of the MIMO form S-parameters.

and AMC structures are adapted in [6], [8] and [10] that increase the footprint of the antenna system. Other simple techniques that are proposed in [18]–[21] effectively reduce the coupling in MIMO DRA without increasing the footprint or height of the antenna. In [18], the metal strips are printed on the top surface of the DRA, whereas high-order modes

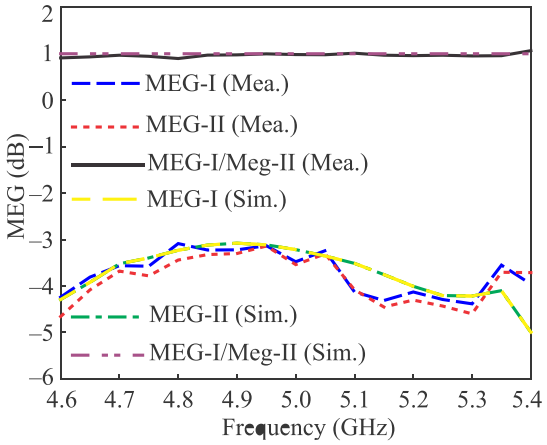

FIGURE 15. Comparison of the simulated and measured MEG of Port-I and Port-II.

in DRA elements are utilized to increase the isolation level is presented in [19]. Unlikely [18], the strips are printed on the lateral walls of the DRA that are shorted with the ground is presented in [20], however, multiple strips are printed on the two adjacent surfaces as well as the farther edges of the MIMO DRA elements is proposed in [21]. Finally, the proposed technique is very simple that comprises a closed metallic loop printed on the edges of the adjacent walls of the DRA elements. The size of the isolating structures (in terms of wavelength) are listed in column 7 in terms of the area or the volume occupied by each isolating structure, which specifies the Edge-to-Edge (E-E) separation of the MIMO elements. The E-E distance in the proposed MIMO DRA elements is only $0.016\lambda_0$, which is the minimum separation achieved. With this compact structure, the measured isolation of 28 dB is realized with a stable radiation pattern for each port and with ECC less than 0.05 over the required band. To Summarize the comparison, the proposed structure is more compact and has fairly good performance in terms of isolation than [5]–[12]. The designs in [18] and [19] are simple and have almost same measured isolation performance, however, the E-E separation is larger between the elements. The designs presented in [20] and [21] provide simulation results only for the isolation in MIMO DRA. An isolation of 28 dB is obtained in [20] with the E-E distance of $0.005\lambda_0$. The isolation mechanism is explained very well, however, it only considers the coupling due to the fields near the lateral walls of the DRA elements. On the contrary, in the proposed design the coupling fields near the lateral walls and in the middle of the DR have been taken into account. Therefore, for fair comparison the simulated value of isolation is to be considered in the proposed design that is –50 dB, which is better than given in [20]. Comparing the performance of the proposed design with [21], an equal level of isolation is realized in both designs. However, the proposed design is more compact that has the small inter-element distance ($0.016\lambda_0$) as compared to $0.0866\lambda_0$ in [21]. Moreover, the radiation pattern in the $\phi = 90°$ is tilted off the broadside direction, whereas, in the proposed design the radiation patterns at both the ports are the mirror image in the $\phi = 0°$ and symmetrical pattern in $\phi = 90°$ plane, which ensures the overall pattern with the peak value directed in the broadside direction. Based on the above comparison, it is clear that proposed technique has superior performance in terms of compactness, isolation, and radiation pattern stability. Besides this, the sensitivity analysis of the decoupling structure and its effect on the MIMO DRA performance is provided with great detail. In addition, the fabrication tolerance is studied by comparing the measured results of the two prototypes, which is lacking in [20] and [21].

V. CONCLUSION

A very simple and compact magnetic loop has been proposed as a decoupler to improve the isolation in MIMO DRAs. A measured isolation level of 28 dB was realized with a stable radiation pattern for each port and low ECC < 0.05 in the Sub–6GHz 5G band. The performance of the proposed design was compared with the conventional design, top strip based design, and with grounded strip based design, which is best among them. Next, the isolation mechanism of the closed metallic loop is illustrated, which shows the effectiveness of the propose technique. Then, sensitivity analysis is studied. Finally, the effect of fabrication tolerance has been verified through simulations and measurements. Moreover, the farfield parameters, i.e., co-pol radiation patterns, ECC, DG, and MEG are measured and have very good agreement with simulation.

REFERENCES

[1] A. Sharma, A. Sarkar, A. Biswas, and M. J. Akhtar, "A-shaped wideband dielectric resonator antenna for wireless communication systems and its MIMO implementation," *Int. J. RF Microw. Comput.-Aided Eng.*, vol. 28, no. 8, Oct. 2018, Art. no. e21402.

[2] A. Sharma, A. Sarkar, A. Biswas, and M. J. Akhtar, "Equilateral triangular dielectric resonator based co-radiator MIMO antennas with dual-polarisation," *IET Microw., Antennas Propag.*, vol. 12, no. 14, pp. 2161–2166, Nov. 2018.

[3] A. Petosa, *Dielectric Resonator Antenna Handbook*. Norwood, MA, USA: Artech House, 2007.

[4] K. M. Luk and K. W. Leung, *Dielectric Resonator Antennas*. Baldock, U.K.: Research Studies Press, 2003.

[5] A. Dadgarpour, B. Zarghooni, B. S. Virdee, T. A. Denidni, and A. A. Kishk, "Mutual coupling reduction in dielectric resonator antennas using metasurface shield for 60-GHz MIMO systems," *IEEE Antennas Wireless Propag. Lett.*, vol. 16, pp. 477–480, 2017.

[6] S. D. Assimonis, T. V. Yioultsis, and C. S. Antonopoulos, "Design and optimization of uniplanar EBG structures for low profile antenna applications and mutual coupling reduction," *IEEE Trans. Antennas Propag.*, vol. 60, no. 10, pp. 4944–4949, Oct. 2012.

[7] M. J. Al-Hasan, T. A. Denidni, and A. Sebak, "Millimeter-wave compact EBG structure for mutual-coupling reduction in dielectric resonator antenna arrays," *IEEE Antennas Propag. Soc. Int. Symp. (APSURSI)*, Jul. 2013, pp. 95–96.

[8] D. Guha, S. Biswas, T. Joseph, and M. T. Sebastian, "Defected ground structure to reduce mutual coupling between cylindrical dielectric resonator antennas," *Electron. Lett.*, vol. 44, pp. 836–837, Jul. 2008.

[9] N. Al Shalaby and S. G. El-Sherbiny, "Mutual coupling reduction of DRA for MIMO applications," *Adv. Electromagn.*, vol. 8, no. 1, pp. 75–81, May 2019.

[10] G. Zheng, A. A. Kishk, A. W. Glisson, and A. B. Yakovlev, "A mutual coupling reduction technique for dielectric resonator antennas over AMC surface," in *Proc. IEEE Antennas Propag. Soc. Int. Symp.*, Albuquerque, NM, USA, Jul. 2006, pp. 377–380.

[11] R. Karimian, A. Kesavan, M. Nedil, and T. A. Denidni, "Low-mutual-coupling 60-GHz MIMO antenna system with frequency selective surface wall," *IEEE Antennas Wireless Propag. Lett.*, vol. 16, pp. 373–376, 2017.
[12] M. Li and S. Cheung, "Isolation enhancement for MIMO dielectric resonator antennas using dielectric superstrate," *IEEE Trans. Antennas Propag.*, vol. 69, no. 7, pp. 4154–4159, Jul. 2021.
[13] A. Hagras, T. A. Denidni, M. Nedil, and Y. Coulibaly, "Low-mutual coupling antenna array for millimeter-wave MIMO applications," in *Proc. IEEE Int. Symp. Antennas Propag.*, Jul. 2012, pp. 1–2.
[14] J.-B. Yan and J. T. Bernhard, "Design of a MIMO dielectric resonator antenna for LTE femtocell base stations," *IEEE Trans. Antennas Propag.*, vol. 60, no. 2, pp. 438–444, Feb. 2012.
[15] L. F. Zou, D. Abbott, and C. Fumeaux, "Omnidirectional cylindrical dielectric resonator antenna with dual polarization," *IEEE Antennas Wireless Propag. Lett.*, vol. 11, pp. 515–518, 2012.
[16] A. Abdalrazik, A. S. A. El-Hameed, and A. B. Abdel-Rahman, "A three-port MIMO dielectric resonator antenna using decoupled modes," *IEEE Antennas Wireless Propag. Lett.*, vol. 16, pp. 3104–3107, 2017.
[17] M. Al-Hasan, I. B. Mabrouk, E. R. F. Almajali, M. Nedil, and T. A. Denidni, "Hybrid isolator for mutual-coupling reduction in millimeter-wave MIMO antenna systems," *IEEE Access*, vol. 7, pp. 58466–58474, 2019, doi: 10.1109/ACCESS.2019.2914902.
[18] Y. Zhang, J.-Y. Deng, M.-J. Li, D. Sun, and L.-X. Guo, "A MIMO dielectric resonator antenna with improved isolation for 5G mm-Wave applications," *IEEE Antennas Wireless Propag. Lett.*, vol. 18, no. 4, pp. 747–751, Apr. 2019.
[19] Y. M. Pan, Y. Hu, and S. Y. Zheng, "Design of low mutual coupling dielectric resonator antennas without using extra decoupling element," *IEEE Trans. Antennas Propag.*, vol. 69, no. 11, pp. 7377–7385, Nov. 2021.
[20] M. Elahi, A. Altaf, J. Yousaf, and E. R. A. Majali, "Isolation improvement in MIMO dielectric resonator antenna," in *Proc. IEEE Int. Symp. Antennas Propag. USNC-URSI Radio Sci. Meeting (APS/URSI)*, Dec. 2021, pp. 1151–1152.
[21] X.-J. Wu, Z. Chen, T. Yuan, and S.-Z. Liu, "A decoupling method for E-plane coupled millimeter-wave MIMO dielectric resonator antennas," in *Proc. Cross Strait Radio Sci. Wireless Technol. Conf. (CSRSWTC)*, Oct. 2021, pp. 109–111.
[22] A. Altaf and M. Seo, "Size-reduction of a dual-band circularly polarized dielectric resonator antennas," *IEEE Access*, vol. 9, pp. 126457–126465, 2021.
[23] A. Altaf and M. Seo, "An electronically-switched frequency-agile hybrid dielectric resonator antenna with a fixed reconfigurable circularly polarized band," *IEEE Access*, vol. 8, pp. 143509–143518, 2020.
[24] S. Blanch, J. Romeu, and I. Corbella, "Exact representation of antenna system diversity performance from input parameter description," *Electron. Lett.*, vol. 39, no. 9, pp. 705–707, May 2003.
[25] M. S. Sharawi, "Current misuses and future prospects for printed multiple-input, multiple-output antenna systems [wireless corner]," *IEEE Antennas Propag. Mag.*, vol. 59, no. 2, pp. 162–170, Apr. 2017.
[26] A. A. Khan, M. H. Jamaluddin, S. Aqeel, J. Nasir, J. U. R. Kazim, and O. Owais, "Dual-band MIMO dielectric resonator antenna for WiMAX/WLAN applications," *IET Microw., Antennas Propag.*, vol. 11, no. 1, pp. 113–120, Jan. 2017.
[27] T. Kumari, G. Das, A. Sharma, and R. K. Gangwar, "Design approach for dual element hybrid MIMO antenna arrangement for wideband applications," *Int. J. RF Microw. Comput.-Aided Eng.*, vol. 29, no. 1, Jan. 2019, Art. no. e21486.

MANZOOR ELAHI (Member, IEEE) received the B.Sc. degree in electrical engineering from the University of Engineering and Technology, Peshawar, Pakistan, the M.S. degree from COMSATS University, Islamabad, Pakistan, in 2011 and 2015, respectively, and the Ph.D. degree in electrical and computer engineering from Sungkyunkwan University, Suwon, South Korea, in 2022. Currently, he is working as a Postdoctoral Researcher with the School of Electrical and Electronic Engineering, Chung-Ang University, Seoul, South Korea. His research interests include MIMO antennas, circularly polarized antennas, reconfigurable dielectric resonator antennas, substrate integrated waveguide antennas, and reflectarray antennas.

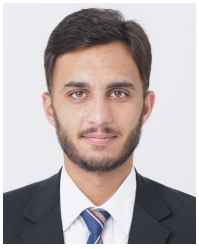

AMIR ALTAF (Member, IEEE) received the B.Sc. degree in electrical engineering from the University of Engineering and Technology, Peshawar, Pakistan, in 2011, and the Ph.D. degree from the Division of Electronics and Electrical Engineering, Dongguk University, Seoul, South Korea, in 2018. Currently, he is working as a Postdoctoral Researcher with the Department of Electrical and Computer Engineering, Sungkyunkwan University, Suwon, South Korea. He has been a recipient of the Prestigious Brain Korea (BK) Postdoctoral Fellowship, since March 2018. His research interests include circularly polarized antennas, reconfigurable antennas, millimeter-wave integrated antennas, modeling of high frequency bondwire interconnects, and active circuits. He is a member of IEEE Antennas and Propagation Society.

EQAB ALMAJALI (Member, IEEE) received the M.A.Sc. and Ph.D. degrees (Hons.) in electrical engineering from the University of Ottawa, Ottawa, ON, Canada, in 2010 and 2014, respectively. He has been an Assistant Professor with the Electrical Engineering Department, University of Sharjah, since August 2018. Prior to that, he worked as a Postdoctoral Fellow with the Electronics Department, Carleton University, Canada. He was awarded the Prestigious Canadian National Science and Engineering Research Council (NSERC) Postdoctoral Fellowship, in 2014, for his research excellence and also was awarded the NSERC-PGS scholarship during his doctoral studies, in 2012. He is the author of over 45 technical publications and a coauthor of two-book chapters published by Artech and Wiley. His current research interests include 5G high-gain MIMO antennas, millimeter wave lenses, low profile metasufrace antennas, and applications of artificial intelligence and machine learning in 5G reflectarrays and trasmitarrays antenna design.

JAWAD YOUSAF received the M.S. and Ph.D. degrees in electronics and electrical engineering from Sungkyunkwan University, Suwon, South Korea, in 2016 and 2019, respectively. He is currently working as an Assistant Professor with the Electrical, Computer, and Biomedical Engineering Department, Abu Dhabi University, United Arab Emirates. Lastly, he worked as a Prestigious Brain of Korea (BK)-Postdoctoral Fellow with the EMC Laboratory, Sungkyunkwan University, from March 2019 to July 2019. Also, he worked as the Senior RF Researcher in the Pakistan Space and Upper Atmosphere Research Commission (SUPARCO: National Space Agency of Pakistan), from 2009 to 2013. His research interests include applications of artificial intelligence in electromagnetics and bio-applications, ESD analysis, reverberation chamber, CP antenna designing and modeling, chipless RFID tags, analysis of socio-economic problems, and EMI/EMC analysis and measurements of the systems for space and commercial environment. His research work has resulted in over 87 publications in leading peer-reviewed international technical journals and refereed international and national conferences. He was a recipient of the Prestigious Brain of Korea (BK)-21 Postdoctoral Fellowship 2019, the 2nd Best Ph.D. Graduate Award of College 2019, the Best Paper Award in 49th KIEE Summer Conference 2018, the Winner of the Grand Prize for Best Paper in 3rd Electromagnetic Measurement Competition of KIESS 2018, the Prestigious Annual EMC Scholarship Award of KIEES and EMCIS Company Ltd., in 2017, the Best EMC Symposium Paper Award and EDCOM Best Student Paper Award Finalist, in 2017, IEEE International Symposium on EMC, and SI/PI 2017, USA.